# InN dielectric function from the midinfrared to the visible range

L. A. Falkovsky
*L.D. Landau Institute for Theoretical Physics, Moscow 117334, Russia*
*and Institute of the High Pressure Physics, Troitsk 142190, Russia*

(Received 12 January 2009; revised manuscript received 20 February 2009; published 30 March 2009)

The dispersion of the dielectric function for wurtzite InN is analytically evaluated in the region near the fundamental energy gap. The real part of the dielectric function has a logarithmic singularity at the absorption edge. This results in the large contribution into the optical dielectric constant. For samples with degenerate carriers, the real part of the dielectric function is divergent at the absorption edge. The divergence is smeared with temperatures or relaxation rate. The imaginary part of the dielectric function has a plateau far away from the absorption onset.

DOI: 10.1103/PhysRevB.79.113203 PACS number(s): 78.20.Ci, 71.15.Mb, 71.20.Nr

Recently, InN has attracted considerable attention due to its potential application as other III nitrides but especially owing to the small energy band gap $2\varepsilon_g$ of about 0.7 eV observed[1–5] in contrast to the value of 1.9 eV established for the last 20 years. The small band-gap value corresponds to a small effective electron mass $m^* \approx 0.07 m_0$.[6–8]

For future progress in the research field, reliable material parameters are derived from the most widespread *ab initio* electronic-structure calculations. However, these methods do not present analytical results and lead sometimes to contradictions,[9] whether the $4d$ bands are included in the core or not. Therefore, the $\mathbf{k}\cdot\mathbf{p}$ Hamiltonian is used to clarify the physical content. In the corresponding Kane model[10] for the wurtzite case, the conduction band and the valence band are constructed from the $|s\rangle$ and $|x\rangle$, $|y\rangle$, and $|z\rangle$ states at the $\Gamma$ point.

The scheme of valence-band splitting in InN under the crystal field $\Delta_{CR}$ and the spin-orbit (SO) interaction $\Delta_{SO}$ is shown in Fig. 1(a). According to experimental data[11] and calculations,[8] this splitting has a value on the order of 0.02–0.06 eV, small in comparison with the band gap, and can be ignored in calculations of the integral properties, such as optical absorption. Therefore, the Kane model can be substantially simplified while using in calculations of the dielectric function (DF).

In this Brief Report with the help of the simplified Kane model, we evaluate analytically the DF for wurtzite InN in the range $\omega \sim 0.3-4$ eV, where absorption is dominated by optical transitions from three highest valence bands into the lowest conduction band. We consider a pristine semiconductor as well as doped semiconductors with carriers. As well known, the imaginary part of the DF has (i) the square-root behavior near the absorption edge in the case where the conduction band is empty and (ii) the steplike behavior in the case where the carriers in the conduction band are degenerate. In Ref. 12 the *ab initio* calculations of the imaginary part were presented for the InN polymorphs (with wurtzite, zinc-blende, and rocksalt structures) in case (i), whereas the real part was restored using the Kramers-Kronig relations. In Ref. 12 the imaginary part was also estimated within the Kane model, but the optical-transition matrix elements were taken in the $k$ independent form that is incorrect for a narrow-gap semiconductor with a large carrier concentration.

We find that the real part of the DF has at the absorption edge the kinklike singularity in case (i) and the logarithmic divergence in case (ii). Such singularities have been previously obtained for graphene[13] and for IV-VI semiconductors.[14] The singularities are smeared with temperatures or carrier relaxation. The excitonic effects were not observed experimentally in InN since they are suppressed by the carrier relaxation (see Refs. 6, 12, and 15 for their estimations).

The effective Hamiltonian of the simplified anisotropic Kane model is given as the matrix $4\times 4$,

$$H = \begin{pmatrix} \varepsilon_g & iP_2k_x & iP_2k_y & iP_1k_z \\ -iP_2k_x & -\varepsilon_g & 0 & 0 \\ -iP_2k_y & 0 & -\varepsilon_g & 0 \\ -iP_1k_z & 0 & 0 & -\varepsilon_g \end{pmatrix}, \qquad (1)$$

where $P_1 \neq P_2$ are the interband momentum-matrix elements with the velocity dimension (we set $\hbar = 1$ in the intermediate formulas). Quadratic terms in momentum $\mathbf{k}$ can be written[16] in the main diagonal of matrix (1), as well as in the terms connecting the states at the valence-band top, $-\varepsilon_g$. We omit them because their contribution in the DF is on the order of $1/\ln(\varepsilon_{at}/\varepsilon_g) \ll 1$, where $\varepsilon_{at}$ is the energy of the atomic scale.

Hamiltonian (1) gives rise to the eigenvalues

$$\varepsilon_{1,4} = \pm[\varepsilon_g^2 + P_1^2k_z^2 + P_2^2k_\perp^2]^{1/2}, \quad k_\perp^2 = k_x^2 + k_y^2, \qquad (2)$$

corresponding to the conduction band and the light-hole band, and the twofold eigenvalue

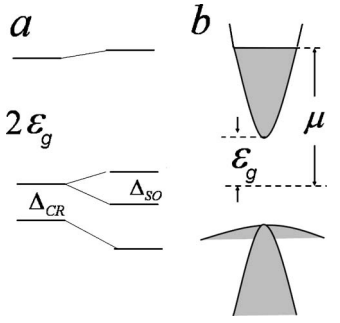


FIG. 1. (a) Scheme of valence-band splitting under the crystal field and SO interactions; (b) conduction, heavy-hole, and light-hole bands near the $\Gamma$ point.

 

$$\varepsilon_{2,3} = -\varepsilon_g \tag{3}$$

for the heavy-hole band [see Fig. 1(b)].

The effective masses at the conduction-band bottom are

$$m_\parallel = \varepsilon_g/P_1^2 \text{ and } m_\perp = \varepsilon_g/P_2^2 \tag{4}$$

for the longitudinal and transverse directions, respectively, to the $z$ axis. Comparison with the values $m_\parallel = 0.065m_0$, $m_\perp = 0.068m_0$, and $2\varepsilon_g = 0.69$ eV obtained[8] in the experimental data analysis gives $P_1 = 0.966 \times 10^8$ cm/sec and $P_2 = 0.945 \times 10^8$ cm/sec.

The velocity operator has the form

$$\mathbf{v} = \frac{\partial H}{\partial \mathbf{k}} = \begin{pmatrix} 0 & iP_2\mathbf{e}_x & iP_2\mathbf{e}_y & iP_1\mathbf{e}_z \\ -iP_2\mathbf{e}_x & 0 & 0 & 0 \\ -iP_2\mathbf{e}_y & 0 & 0 & 0 \\ -iP_1\mathbf{e}_z & 0 & 0 & 0 \end{pmatrix},$$

with orthonormal vectors $\mathbf{e}_j$ chosen along the coordinate axes.

Let us define the velocity matrix in the representation diagonalizing Hamiltonian (1),

$$\tilde{\mathbf{v}} = U^\dagger \mathbf{v} U.$$

Using the eigenfunctions of the Hamiltonian, one finds the matrix $U$,

$$U = \begin{pmatrix} -a_1 & 0 & 0 & a_2 \\ ip_x/n_1 & -p_y/p_\perp & p_x p_z/p_\perp p & ip_x/n_2 \\ ip_y/n_1 & p_x/p_\perp & p_y p_z/p_\perp p & ip_y/n_2 \\ ip_z/n_1 & 0 & -p_\perp/p & ip_z/n_2 \end{pmatrix},$$

where $p_z = P_1 k_z$, $p_{x,y} = P_2 k_{x,y}$, $p = \sqrt{p_z^2 + p_\perp^2}$, $n_{1,2} = \sqrt{2\varepsilon_1(\varepsilon_1 \pm \varepsilon_g)}$, and $a_{1,2} = \sqrt{(\varepsilon_1 \pm \varepsilon_g)/2\varepsilon_1}$, and $\varepsilon_1$ is given in Eq. (2).

We note that the diagonal velocity-matrix elements in this representation coincide with the derivative of the eigenvalues

$$\langle i|\tilde{\mathbf{v}}|i\rangle = \frac{\partial \varepsilon_i}{\partial \mathbf{k}},$$

and we find the off-diagonal elements as follows:

$$\langle 1|\tilde{\mathbf{v}}|2\rangle = i\sqrt{\frac{\varepsilon_1 + \varepsilon_g}{2\varepsilon_1}} P_2 \frac{k_y\mathbf{e}_x - k_x\mathbf{e}_y}{k_\perp},$$

$$\langle 1|\tilde{\mathbf{v}}|3\rangle = \frac{-iP_1P_2}{\sqrt{2\varepsilon_1(\varepsilon_1 - \varepsilon_g)}}\left[\frac{k_z}{k_\perp}(k_x\mathbf{e}_x + k_y\mathbf{e}_y) - k_\perp\mathbf{e}_z\right],$$

$$\langle 1|\tilde{\mathbf{v}}|4\rangle = \frac{\varepsilon_g}{\varepsilon_1\sqrt{\varepsilon_1^2 - \varepsilon_g^2}}(P_1^2 k_z\mathbf{e}_z + P_2^2 k_x\mathbf{e}_x + P_2^2 k_y\mathbf{e}_y),$$

$$\langle 3|\tilde{\mathbf{v}}|4\rangle = \frac{-iP_1P_2}{\sqrt{2\varepsilon_1(\varepsilon_1 + \varepsilon_g)}}\left[\frac{k_z}{k_\perp}(k_x\mathbf{e}_x + k_y\mathbf{e}_y) - k_\perp\mathbf{e}_z\right]. \tag{5}$$

These matrix elements are involved in the general quantum-mechanic formula for the dynamic conductivity $\sigma_{\alpha\beta}(\omega)$ derived in Ref. 13. Then, we obtain the DF with the help of the relation

$$\epsilon_{\alpha\beta}(\omega) = 1 + 4\pi i\sigma_{\alpha\beta}(\omega)/\omega. \tag{6}$$

Due to the symmetry, the off-diagonal tensor components of the DF vanish, and there are only two independent components $\epsilon_{zz}(\omega)$ and $\epsilon_{xx}(\omega) = \epsilon_{yy}(\omega)$.

The DF is separated into intraband and interband parts. The intraband term contains only the diagonal velocity-matrix elements and has the Drude-Boltzmann form. For instance, we obtain for the intraband contribution of degenerate carriers in the conduction band,

$$\epsilon_{zz}^{\text{intra}}(\omega) = -\frac{4e^2P_1}{3\pi\hbar P_2^2}\frac{(\mu^2 - \varepsilon_g^2)^{3/2}}{\omega(\omega + i\nu)\mu}, \tag{7}$$

where the chemical potential $\mu$, the relaxation rate $\nu$, and the photon frequency $\omega$ are written in the common units.

Neglecting the carrier relaxation, we can write the interband term for the extraordinary component of the DF in the form

$$\epsilon_{zz}^{\text{inter}}(\omega) = 1 + \frac{2e^2}{\pi^2}\int d^3k \left\{ \frac{[f(-\varepsilon_1) - f(\varepsilon_1)]|\tilde{v}_{14}^z|^2}{2\varepsilon_1[4\varepsilon_1^2 - (\omega + i\delta)^2]} + \frac{[f(-\varepsilon_g) - f(\varepsilon_1)]|\tilde{v}_{13}^z|^2}{(\varepsilon_1 + \varepsilon_g)[(\varepsilon_1 + \varepsilon_g)^2 - (\omega + i\delta)^2]} + \frac{[f(-\varepsilon_1) - f(-\varepsilon_g)]|\tilde{v}_{34}^z|^2}{(\varepsilon_1 - \varepsilon_g)[(\varepsilon_1 - \varepsilon_g)^2 - (\omega + i\delta)^2]} \right\}, \tag{8}$$

where $f(\varepsilon) = 1/\{\exp[(\varepsilon - \mu)/T] - 1\}$ is the Fermi function. For the pristine semiconductor at low temperature, the conduction band is empty, but in the case of $n$-type doping, the chemical potential $\mu$ is higher than the conduction-band bottom $\varepsilon_g$ [see Fig. 1(b)].

The different terms in the braces present the various optical transitions; first, between the light-hole band and the conduction band; second, between the heavy-hole band and the conduction band; and third, between the light- and heavy-hole bands. The infinitesimal $\delta$ in the denominators of Eq. (8) defines the bypass around the poles. These bypasses give the imaginary part of the DF, whereas the principal values of the integrals yield the real part.

Transforming the integration variables

$$k_x = \frac{\sqrt{\varepsilon_1^2 - \varepsilon_g^2}}{P_2}\sin\theta\cos\varphi, \quad k_y = \frac{\sqrt{\varepsilon_1^2 - \varepsilon_g^2}}{P_2}\sin\theta\sin\varphi,$$

$$k_z = \frac{\sqrt{\varepsilon_1^2 - \varepsilon_g^2}}{P_1}\cos\theta, \quad \frac{\partial(k_z, k_x, k_y)}{\partial(\varepsilon_1, \theta, \varphi)} = \frac{\varepsilon_1\sqrt{\varepsilon_1^2 - \varepsilon_g^2}}{P_1P_2^2}\sin\theta, \tag{9}$$

we integrate over the angles $\theta$ and $\varphi$,

$$\epsilon_{zz}^{\text{inter}}(\omega) = \frac{8e^2P_1}{3\pi\hbar P_2^2}\int_{\varepsilon_g}^{\varepsilon_{\text{at}}} d\varepsilon\sqrt{\varepsilon^2 - \varepsilon_g^2}\left\{ \frac{\varepsilon_g^2[f(-\varepsilon) - f(\varepsilon)]}{2\varepsilon^2[4\varepsilon^2 - (\omega + i\delta)^2]} + \frac{f(-\varepsilon_g) - f(\varepsilon)}{(\varepsilon + \varepsilon_g)^2 - (\omega + i\delta)^2} + \frac{f(-\varepsilon) - f(-\varepsilon_g)}{(\varepsilon - \varepsilon_g)^2 - (\omega + i\delta)^2} \right\} + 1.$$

The integral presenting the real part of the DF diverges logarithmically at the upper limit. Since the leading contri-

bution arises from the values $\varepsilon \sim (\mu, \omega)$, we can cutoff the integral at the atomic energy $\varepsilon_{\rm at}$, where our linear $\mathbf{k}\cdot\mathbf{p}$ expansion becomes incorrect. The imaginary part is easily evaluated for zero temperatures. For instance, we find for the case $\mu > \varepsilon_g$, when electrons fill the conduction band,

$$\mathrm{Im}\ \epsilon_{zz}^{\rm inter}(\omega) = \frac{4e^2P_1}{3\hbar P_2^2}\left\{\frac{\varepsilon_g^2}{2\omega^2}\sqrt{1-\frac{(2\varepsilon_g)^2}{\omega^2}}\theta(\omega-2\mu) + \sqrt{1-\frac{2\varepsilon_g}{\omega}}\theta(\omega-\varepsilon_g-\mu)\right\}, \tag{10}$$

where the step $\theta$ function conveys the condition for the interband electron absorption.

Let us emphasize that for doped semiconductor, the band edge at $\omega=2\mu$ for the optical transitions into the conduction band from the light-hole band is higher than the edge for the transition from the heavy-hole band at $\omega=\varepsilon_g+\mu$. With increasing the free-carrier concentration, both edges demonstrate the blue Burstein-Moss shift. At zero temperatures, the chemical potential $\mu$, measured from the midgap, is determined by the free-carrier concentration $n_0=(\mu^2-\varepsilon_g^2)^{3/2}/3\pi^2\hbar^3P_1P_2^2$.

If the carriers are absent in the conduction band, $-\varepsilon_g < \mu < \varepsilon_g$, the imaginary part of the DF is given in Eq. (10) with substitution $\mu \to \varepsilon_g$. Far away from the absorption edges, where $\omega \gg \varepsilon_g+\mu$, the imaginary part demonstrates the plateaulike character with

$$\max\ \mathrm{Im}\ \epsilon^{\rm inter}(\omega) = \frac{4e^2P_1}{3\hbar P_2^2}. \tag{11}$$

The plateau noticed also in Ref. 12 and for the $A_4B_6$ semiconductors in Ref. 14 is a consequence of the linearity of the electron dispersion at the energy that is larger in comparison with the energy gap.

The real part of the DF contains the following contributions. The transitions between the heavy-hole bands and the conduction band give

$$\mathrm{Re}\ \epsilon_{zz}^{c,hh}(\omega) = \frac{8e^2P_1}{3\pi\hbar P_2^2}\left\{\ln\frac{2\varepsilon_{\rm at}}{\mu+\sqrt{\mu^2-\varepsilon_g^2}} + \frac{\sqrt{1+2x}}{2}\ln\frac{\mu+(\mu+\varepsilon_g)x+\sqrt{(\mu^2-\varepsilon_g^2)(1+2x)}}{(\mu+\varepsilon_g+\omega)(1+x+\sqrt{1+2x})} + F(x)\right\}, \tag{12}$$

where

$$F(x) = \frac{\sqrt{1-2x}}{2}\ln\frac{\mu-(\mu+\varepsilon_g)x+\sqrt{(\mu^2-\varepsilon_g^2)(1-2x)}}{|\omega-\mu-\varepsilon_g|(1-x+\sqrt{1-2x})} \tag{13}$$

if $x=\varepsilon_g/\omega < 1/2$ and

$$F(x) = -\sqrt{2x-1}\ \arctan\frac{\omega\sqrt{2x-1}}{\mu+\varepsilon_g-\omega+\sqrt{\mu^2-\varepsilon_g^2}}$$

if $x > 1/2$.

The transitions between the light-hole band and the conduction band contribute

$$\mathrm{Re}\ \epsilon_{zz}^{c,\rm lh}(\omega) = \frac{4e^2P_1x^2}{3\pi\hbar P_2^2}\left\{1-\sqrt{1-\varepsilon_g^2/\mu^2} + \sqrt{1-4x^2}\ \ln\frac{\sqrt{\mu^2-\varepsilon_g^2}+\mu\sqrt{1-4x^2}}{|(\omega/2)^2-\mu^2|^{1/2}(1+\sqrt{1-4x^2})}\right\} \tag{14}$$

for $x < 1/2$ and

$$\mathrm{Re}\ \epsilon_{zz}^{c,\rm lh}(\omega) = \frac{4e^2P_1x^2}{3\pi\hbar P_2^2}\left\{1-\sqrt{1-\varepsilon_g^2/\mu^2} - \sqrt{4x^2-1}\ \arctan\frac{(1-\sqrt{1-\varepsilon_g^2/\mu^2})\sqrt{4x^2-1}}{\sqrt{1-\varepsilon_g^2/\mu^2-1+4x^2}}\right\} \tag{15}$$

for $x > 1/2$.

We find that the real part of the DF as a function of $\omega$ takes at $x=1/2$ the maximal value for $\mu=\varepsilon_g$,

$$\max\ \mathrm{Re}\ \epsilon_{zz}^{\rm inter} = 1 + \frac{8e^2P_1}{3\pi\hbar P_2^2}\left[\ln\frac{2\varepsilon_{\rm at}}{\varepsilon_g} - \frac{\ln(3+2\sqrt{2})}{\sqrt{2}} + \frac{1}{8}\right]. \tag{16}$$

If the carriers appear in the conduction band, $\mu > \varepsilon_g$, the real part of the DF has a logarithmic singularity which can be smeared with temperature or carrier relaxation. For the relaxation rate $\nu$, which is small in comparison with the photon frequency $\omega$, we have in Eqs. (10), (13), and (14) to substitute

$$\theta(\omega-\omega_{\rm at}) \to \frac{1}{2}+\frac{1}{\pi}\arctan[(\omega-\omega_{\rm at})/2\nu],$$

$$(\omega-\omega_{\rm at})^2 \to (\omega-\omega_{\rm at})^2+(2\nu)^2, \tag{17}$$

where $\omega_{\rm at}$ is the absorption edge equal to $\varepsilon_g+\mu$ or $2\mu$ for the corresponding transitions. If temperature plays a more important role, calculations show that we should place $T$ instead of $\nu$ in Eq. (17).

So far the extraordinary component $\epsilon_{zz}$ was presented. The ordinary component $\epsilon_{xx}$ differs only in the factor $P_2/P_1$, which equals 0.98 for the experimental values of the effective masses in Eq. (4).

Now the value of the cutoff parameter $\varepsilon_{\rm at}$ is only needed to calculate the DF. To estimate this value, we can use the energy arising in the Kane model while the quadratic terms are taken into account. According to estimations,[8,12] this energy ranges from 8 to 15 eV. We take the intermediate value $\varepsilon_{\rm at}=10$ eV by plotting Fig. 2, where our theoretical results are shown. The maximum value of the real part, Eq. (16), is found to be equal to 6.91 and the imaginary part of the DF takes the value 3.16 on the plateau, Eq. (11). The corresponding values, 2.5–3.5, obtained from experiments[17–19] and calculated from the first principles[12] are on the plateau in the frequency range 1.5–4.0 eV. This agrees very well with Fig. 2 (right panel). The experiment[18] finds a value of about

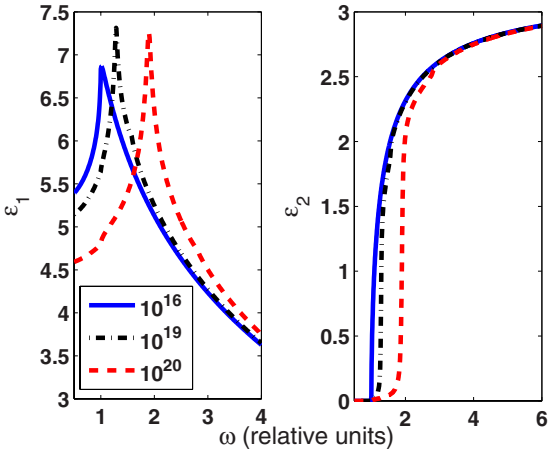


FIG. 2. (Color online) The real and imaginary parts of the DF versus the photon frequency (in units of the gap $2\varepsilon_g=0.69$ eV) for various free-electron concentrations; corresponding values of the chemical potential $\mu$ are 1.01, 1.57, and 2.79 (in units of $2\varepsilon_g$); relaxation rate is $\nu=0.01\mu$.

$\simeq 9$ for the maximum of the real part. The estimation[18] of the dielectric constant gives $\epsilon_\infty=6.7$. The *ab initio* calculations[12,20] found correspondingly in these two papers $\epsilon_\infty(xx)=7.03$ and 7.16, as well as $\epsilon_\infty(zz)=7.41$ and 7.27. The agreement with our Fig. 2 (left panel) is excellent again. In our calculations, the maximum of the real part for the large carrier concentration increases logarithmically with decreasing of the relaxation rate. Plotting Fig. 2, we take $\nu=0.01\mu$ for various carrier concentrations.

Concerning the dielectric constant $\epsilon_\infty$, we keep in mind that the phonons give a small contribution into its value. This contribution can be estimated as $\omega_{\mathrm{TO}}^2/\omega^2$, where $\omega_{\mathrm{TO}}$ is the transverse phonon frequency which is much less than the photon frequency considered here. Therefore, the phonon contribution into $\epsilon_\infty$ should be considered as negligible.

In conclusion, we find analytically that the real part of the DF contains a singular contribution from the interband optical transitions. It presents the large logarithmic term to the optical dielectric constant. While increasing the frequency, we obtain the dispersion of the dielectric function. Near the edge of the interband absorption, a peak appears in the real part of the DF for degenerate electrons filled the conduction band if the relaxation rate is small enough.

This work was supported by the Russian Foundation for Basic Research (Grant No. 07-02-00571). The author is grateful to the Max Planck Institute for the Physics of Complex Systems for hospitality in Dresden.

[1] V. Y. Davydov, A. A. Klochikhin, R. P. Seisyan, V. V. Emtsev, S. I. Ivanov, F. Bechstedt, J. Furthmüller, H. Harima, A. V. Mudryi, J. Aderhold, O. Semchinova, and J. Graul, Phys. Status Solidi B **229**, R1 (2002).

[2] J. Wu, W. Walukiewicz, K. M. Yu, J. W. Agler III, E. E. Haller, H. Lu, W. J. Schaff, Y. Saito, and Y. Nanishi, Appl. Phys. Lett. **80**, 3967 (2002).

[3] Y. Nanishi, Y. Saito, and T. Yamaguchi, Jpn. J. Appl. Phys., Part 1 **42**, 2549 (2003).

[4] A. Sher, M. van Schilfgaarde, M. A. Berding, S. Krishnamurthy, and A.-B. Chen, MRS Internet J. Nitride Semicond. Res. **4S1**, G5.1 (1999).

[5] F. Bechstedt and J. Furthmüller, J. Cryst. Growth **246**, 315 (2002).

[6] J. Wu, W. Walukiewicz, W. Shan, K. M. Yu, J. W. Ager, E. E. Haller, H. Lu, and W. J. Schaff, Phys. Rev. B **66**, 201403(R) (2002).

[7] S. P. Fu and Y. F. Chen, Appl. Phys. Lett. **85**, 1523 (2004).

[8] Patrick Rinke, M. Winkelnkemper, A. Qteish, D. Bimberg, J. Neugebauer, and M. Scheffler, Phys. Rev. B **77**, 075202 (2008).

[9] D. Bagayoko, L. Franklin, H. Jin, and G. L. Zhao, Phys. Rev. B **76**, 037101 (2007).

[10] E. O. Kane, J. Phys. Chem. Solids **1**, 249 (1957); E. O. Kane, in *Band Theory and Transport Properties: Handbook on Semiconductors*, edited by W. Paul (North-Holland, Amsterdam, 1982), Vol. 1, p. 195.

[11] R. Goldhahn, P. Schley, A. Winzer, M. Rakel, C. Cobet, N. Esser, H. Lu, and W. Schaff, J. Cryst. Growth **288**, 273 (2006).

[12] J. Furthmüller, P. H. Hahn, F. Fuchs, and F. Bechstedt, Phys. Rev. B **72**, 205106 (2005).

[13] L. A. Falkovsky and A. A. Varlamov, Eur. Phys. J. B **56**, 281 (2007); L. A. Falkovsky and S. S. Pershoguba, Phys. Rev. B **76**, 153410 (2007).

[14] L. A. Falkovsky, Phys. Rev. B **77**, 193201 (2008).

[15] J. S. Thakur, Y. V. Danylyuk, D. Haddad, V. M. Naik, R. Naik, and G. W. Auner, Phys. Rev. B **76**, 035309 (2007).

[16] S. L. Chuang and C. S. Chang, Phys. Rev. B **54**, 2491 (1996).

[17] R. Goldhahn, S. Shokovets, V. Cimalla, L. Spiess, G. Ecke, O. Ambacher, J. Furthmüller, F. Bechstedt, H. Lu, and W. J. Schaff, in *GaN and Related Alloys—2002*, edited by C. Wetzel *et al.*, MRS Symposia Proceedings No. 743 (Materials Research Society, Warrendale, PA, 2003), p. L5.9.

[18] A. Kasic, E. Valcheva, B. Monemar, H. Lu, and W. J. Schaff, Phys. Rev. B **70**, 115217 (2004).

[19] R. Goldhahn, A. T. Winzer, V. Cimalla, O. Ambacher, C. Cobet, W. Richter, N. Esser, J. Furthmüller, F. Bechstedt, H. Lu, and W. J. Schaff, Superlattices Microstruct. **36**, 591 (2004).

[20] N. E. Christensen and I. Gorczyca, Phys. Rev. B **50**, 4397 (1994).